Journal of Computational Physics 363 (2018) 11–29

Contents lists available at ScienceDirect

Journal of Computational Physics

www.elsevier.com/locate/jcp

Unified solver for fluid dynamics and aeroacoustics in isentropic gas flows

Arnau Pont [a,b,*], Ramon Codina [a,b], Joan Baiges [a], Oriol Guasch [c]

[a] Universitat Politècnica de Catalunya, Jordi Girona 1-3, Edifici C1, Campus Nord UPC, 08034 Barcelona, Catalonia, Spain
[b] Centre Internacional de Mètodes Numèrics en Enginyeria (CIMNE), Gran Capità s/n, 08034 Barcelona, Catalonia, Spain
[c] GTM Grup de recerca en Tecnologies Mèdia, La Salle, Universitat Ramon Llull. C/Quatre Camins 30, 08022 Barcelona, Catalonia, Spain

ARTICLE INFO

Article history:
Received 6 July 2017
Received in revised form 5 December 2017
Accepted 14 February 2018
Available online 21 March 2018

Keywords:
Isentropic flow
Computational aeroacoustics
Finite elements
Weak imposition of boundary conditions

ABSTRACT

The high computational cost of solving numerically the fully compressible Navier–Stokes equations, together with the poor performance of most numerical formulations for compressible flow in the low Mach number regime, has led to the necessity for more affordable numerical models for Computational Aeroacoustics. For low Mach number subsonic flows with neither shocks nor thermal coupling, both flow dynamics and wave propagation can be considered isentropic. Therefore, a joint isentropic formulation for flow and aeroacoustics can be devised which avoids the need for segregating flow and acoustic scales. Under these assumptions density and pressure fluctuations are directly proportional, and a two field velocity-pressure compressible formulation can be derived as an extension of an incompressible solver. Moreover, the linear system of equations which arises from the proposed isentropic formulation is better conditioned than the homologous incompressible one due to the presence of a pressure time derivative. Similarly to other compressible formulations the prescription of boundary conditions will have to deal with the backscattering of acoustic waves. In this sense, a separated imposition of boundary conditions for flow and acoustic scales which allows the evacuation of waves through Dirichlet boundaries without using any tailored damping model will be presented.

1. Introduction

The compressibility behind the acoustics in Computational Fluid Dynamics (CFD) has been widely treated for several purposes along the history of numerical methods. Towards the 70's, the artificial compressibility method introduced in [1] was developed with the objective of reducing the computational cost of solving the incompressible Navier–Stokes equations in 3D domains. In this framework, the artificially added compressibility through a density or pressure perturbation term was not only a numerical artifact, but a term that could be easily associated to the acoustics of a low speed compressible flow. However, the artificial compressibility method did not aim to describe the acoustic scales of the flow, but to introduce a numerical relaxation parameter which allowed an easier fulfillment of the continuity condition. The main modification of the incompressible Navier–Stokes consisted in adding an artificial time derivative of the pressure to the dimensionless continuity equation, which improved the condition number of the final system to be solved. A similar method was later applied by [2] to the low speed compressible Navier Stokes equations, in which a time derivative of the primitive variables

* Corresponding author at: Universitat Politècnica de Catalunya, Jordi Girona 1-3, Edifici C1, Campus Nord UPC, 08034 Barcelona, Catalonia, Spain.
E-mail addresses: apont@cimne.upc.edu (A. Pont), ramon.codina@upc.edu (R. Codina), joan.baiges@upc.edu (J. Baiges), oguasch@salleurl.edu (O. Guasch).

https://doi.org/10.1016/j.jcp.2018.02.029
0021-9991/

was added to the energy equation in order to reduce the big disparity between the flow velocity and the sound speed. The Chorin method was extended for both incompressible and slow compressible flows by [3] by adding similar terms to all equations in order to obtain a symmetric hyperbolic problem. In other cases such as low Mach number (M) compressible flows, the goal consisted precisely in going in the opposite direction and identifying the acoustic scales of the flow in order to remove them from the problem (see [4]), because they led to an ill-conditioning of the system and to the backscattering of sound waves into the computational domain.

While the addition of a certain amount of compressibility has made the calculation of incompressible flows easier without taking into account the consequent acoustic field, the inclusion of compressibility in the flow formulation has been a drawback for calculating acoustics when dealing with low speed flows. The conservative compressible flow equations are considered the complete representation of the aeroacoustic problem because they describe directly all flow and acoustic scales without any need for modeling, which in terms of Computational Fluid Dynamics (CFD) is called Direct Numerical Simulation (DNS) [5], and in acoustics is referred as Direct Noise Computation (DNC) [6]. However, as stated above, this formulation performs poorly for Mach numbers tending to zero due to the huge difference between flow velocity and wave propagation speed, which causes convergence problems. In order to avoid the bad conditioning of the problem, a series of hybrid methods, which segregate the acoustics from the CFD, were developed. The so called acoustic analogies resolve the acoustic scales by means of an inhomogeneous wave equation where the source term that represents the aerodynamic noise comes from a previous flow calculation. The pioneer work in this field is presented in [7]. This method has been progressively extended to include diffraction by solid boundaries [8] and moving surfaces [9]. Other hybrid methods, such as the incompressible-acoustic split method presented in [10,11] enrich the incompressible flow equations with a variable density linked to pressure perturbations. Then, the time derivative of this perturbed density is translated into isentropic fluctuations of velocity and pressure that are propagated using a purely acoustic compressible solver after subtracting the incompressible component of the flow field. In a similar way, some formulations propagate the near field flow information to the far field with the Linearized Euler Equations (LEE) [12–14] or with the acoustic perturbation equations [15–17], which consist in an acoustic filtering of the LEE source term. All these methods allow a considerable flexibility, for example the use of a different discretization for each problem, as well as different flow and acoustic models. However, these models are based on assumptions and the subsequent approximation errors need to be properly assessed. In some cases, acoustic source terms need to be modeled and might not be straightforward to implement in a finite element code. Moreover, the segregated calculation of flow and acoustic components only assumes a one-way coupling from flow to acoustics, but not the other way around.

The formulation proposed in this work aims for a simplification of Computational Aeroacoustics (CAA) of isentropic compressible flows and proposes a general framework that can be applied to any geometry, spatial discretization or flow regime below the transonic range. It consists in a compressible formulation with primitive variables without solving for the energy equation, since the flow is considered to be isentropic, which after condensing the density field becomes a system of equations in terms of the velocity and the pressure, like in incompressible flow solvers. As a consequence, the implementation cost is very low when one departs from an already implemented incompressible flow solver. Also, the computational cost is reduced with respect to other methodologies due to the following reasons: getting rid of the fully compressible approach and solving only for velocity and pressure, solving all scales at once without acoustic analogies and improving the condition number of the system for the incompressible limit. This formulation provides two important advantages respect to the acoustic analogies and other hybrid methods presented in the previous paragraph: first, it takes into account the acoustic feedback on the flow scales and second, the validity of the acoustic field will not depend on the motion of the flow or the presence of obstacles. These are precisely the main advantages of a DNC. In fact, for flows with $M \to 0$ this solver should converge to the solution of a DNC, but with a much lower computational cost. The only drawback of such a unified system will be, again like in a DNC, the lack of visualization of the acoustic fluctuations at the near field, where the aerodynamic scales are totally dominant and the wave propagation cannot be extracted like in [18] or [19]. As in all compressible flow models, an adequate equation of state needs to be chosen, in this case relating only density and pressure. For simplicity the ideal gas law has been used to close the problem, but the formulation can be easily extended to any other equation of state.

Since the present paper aims at solving both aerodynamics and acoustics scales in a single calculation, the prescription of compatible and accurate boundary conditions for both components of the solution has been an important aspect of this work. From a numerical point of view, the imposition of boundary conditions can be performed as in the incompressible case, avoiding the difficulties found in compressible flows. However, omitting the acoustic scales in the treatment of the external boundaries leads to undesired wave reflections which affect the accuracy and the stability of the unified solver. Therefore, a new method including the combined imposition of essential boundary conditions in a weak sense on the mean flow variables [20], and a Sommerfeld boundary condition for the acoustic component of the pressure will be presented [21]. This combination will allow the acoustic wave to leave the domain through boundaries where the mean flow has been prescribed a certain boundary condition.

As stated above, the present formulation has been implemented as an update of an already existent FEM incompressible flow solver, but is not restricted to this numerical framework. In fact, [22] presents a CAA formulation based on the Lattice–Boltzmann Method (LLM) for isentropic flows, although in this case flow and acoustic scales are segregated. Linear elements have been used for simplicity, but the method can be also automatically applied to high-order grids leading to a decrease of the approximation error, as long as the chosen element is stable. In this sense, stability is provided by the

Variational Multiscale Method (VMS), which in turn models the scales that are not captured by the spatial discretization (subgrid scales) in form of turbulent dissipation [23,24].

The paper is organized as follows: a detailed presentation of the isentropic compressible equations is shown in Section 2. The details of the aforementioned prescription of boundary conditions are presented in Section 3, and the stabilized time-discrete finite element formulation is derived in Section 4. Finally, numerical results are presented in Section 5: three cases consisting in a 2D flow around a cylinder, a 3D flow around an airfoil and a 2D open cavity will be presented and benchmarked against the Lighthill analogy [7] with incompressible flow, the Ffowcs Williams Hawkings (FWH) acoustic analogy [9] using compressible flow and a DNS, respectively. This analysis will allow to show the performance of the present method in its whole application range.

2. Problem formulation

2.1. The differential problem

The present work focuses in the study of the aerodynamic and acoustic behavior of an ideal gas undergoing a reversible thermodynamical process, which is a realistic hypothesis in most aeroacoustic problems without heat transfer or shocks. This initial assumption allows a drastic simplification of the compressible Navier–Stokes equations, since the energy equation does not need to be solved and the primitive variables of the problem can be used. Moreover, a general formulation can be derived for both slow and high speed isentropic flows taking into account the following equalities (see e.g. [25]):

$$\frac{p_0}{p} = \left(1 + \frac{\gamma - 1}{2}\mathrm{M}^2\right)^{\frac{\gamma}{\gamma-1}}, \tag{1}$$

$$\frac{\rho_0}{\rho} = \left(1 + \frac{\gamma - 1}{2}\mathrm{M}^2\right)^{\frac{1}{\gamma-1}}, \tag{2}$$

where γ is the adiabatic constant of the gas, p and ρ are the total pressure and density fields including perturbations caused by the compressibility of the medium, whereas p_0 and ρ_0 are the same fields at stagnation conditions [25]. M is the Mach number, defined as:

$$\mathrm{M} := \frac{|\mathbf{u}|}{c_0}, \tag{3}$$

where $|\mathbf{u}|$ is either the modulus of the pointwise velocity (or a characteristic value of it if one wants to define a global Mach number) and c_0 is the speed of sound in an ideal gas, defined as $c_0 = \sqrt{\frac{\gamma R T_0}{\mathcal{M}}}$, where T_0 is the temperature field at stagnation, R [J/K-mol] is the universal gas constant and $\mathcal{M}$ [kg/mol] is the molar mass of the gas. From Eq. (2) the following equality between ρ and p can be easily obtained:

$$\frac{p_0}{p} = \left(\frac{\rho_0}{\rho}\right)^{\gamma}. \tag{4}$$

Then, differentiating with respect to time both sides of Eq. (4) and using the equation of state for an ideal gas, $p_0 = \frac{\rho_0 R T_0}{\mathcal{M}}$, the next expression connecting pressure and density time derivatives can be found:

$$\partial_t p = \frac{p_0}{\rho_0}\gamma\left(1 + \frac{\gamma - 1}{2}\mathrm{M}^2\right)^{-1}\frac{\partial \rho}{\partial t} = \frac{R T_0}{\mathcal{M}}\gamma\left(1 + \frac{\gamma - 1}{2}\mathrm{M}^2\right)^{-1}\partial_t \rho. \tag{5}$$

The final time derivative of the equation of state for a low speed gas flow can be approximated as

$$\partial_t p \approx c_0^2 \partial_t \rho, \tag{6}$$

the approximation error being $\mathcal{O}\left(\mathrm{M}^2\right)$. Otherwise the speed of sound c has to be computed as follows:

$$c^2 = c_0^2\left(1 + \frac{\gamma - 1}{2}\mathrm{M}^2\right)^{-1}, \tag{7}$$

and then the following equation can be used:

$$\partial_t p = c^2 \partial_t \rho. \tag{8}$$

The same procedure can be applied to the pressure gradient, obtaining the same relationship with respect to the density gradient. This explicit connection between pressure and density variations allows one to greatly simplify the compressible Navier–Stokes equations, since density perturbations can be expressed in terms of pressure. It is important to highlight that

the limit $\mathrm{M} \to 0$ will lead to a problem which will be very similar to the one resulting from the artificial compressibility method and will contain the acoustic scales of the flow. This is remarkable if it is compared to other non-isentropic formulations for low Mach numbers (see for instance [26]), where density variations are linked exclusively to temperature oscillations, and as a consequence no acoustics are captured.

Let us consider a computational domain $\Omega \subset \mathbb{R}^d$ (where $d = 2, 3$ is the number of space dimensions) with a domain boundary $\Gamma = \partial\Omega$ and let $(0, T)$ be the time interval of analysis. The isentropic compressible equations are then:

$$\rho \partial_t \mathbf{u} + \rho \left(\mathbf{u} \cdot \nabla\right) \mathbf{u} - \mu \nabla^2 \mathbf{u} - \frac{1}{3} \mu \nabla \left(\nabla \cdot \mathbf{u}\right) + \nabla p = \mathbf{0} \text{ in } \Omega, \tag{9}$$

$$\partial_t \rho + \mathbf{u} \cdot \nabla \rho + \rho \nabla \cdot \mathbf{u} = 0 \text{ in } \Omega, \tag{10}$$

where $\mathbf{u}$ is the velocity and μ the dynamic viscosity. Boundary and initial conditions need to be appended to this problem. Using Eq. (5) $\partial_t \rho$ can be expressed in terms of $\partial_t p$ and the continuity equation becomes

$$\frac{1}{c^2} \partial_t p + \frac{1}{c^2} \mathbf{u} \cdot \nabla p + \rho \nabla \cdot \mathbf{u} = 0 \text{ in } \Omega, \tag{11}$$

where $c\left(\mathbf{x}, t\right)$ is given by Eq. (7) and $\mathbf{x}$ is the spatial coordinate vector. Despite all simplifications, the previous equation still depends on the function c and two density dependent terms remain in the momentum equation. Calculating these two fields as implicit functions of $[\mathbf{u}, p]$ would increase the complexity of the new scheme with new non-linearities. In this sense, equations (2) and (7) will be used for closing the problem and obtaining a formulation which only depends on the velocity and pressure fields.

2.2. Weak formulation

The next step consists in deriving the variational formulation of the previous problem. Let us denote with $\langle \cdot, \cdot \rangle_\omega$ the integral of the product of two functions in the domain ω, with the subscript omitted when $\omega = \Omega$. Let V and Q be the functional spaces where for each time t the velocity and pressure solutions live, respectively, with appropriate regularity that we will not analyze here. Then, defining the velocity and pressure test functions $\mathbf{v} \in V$ and $\rho q \in Q$, the variational formulation can be written in terms of the forms:

$$\begin{aligned} B([\mathbf{u}, p], [\mathbf{v}, \rho q]) =& \langle \rho \mathbf{v}, \partial_t \mathbf{u} \rangle + \langle \rho \mathbf{v}, \left(\mathbf{u} \cdot \nabla\right) \mathbf{u} \rangle + \mu \langle \nabla \mathbf{v}, \nabla \mathbf{u} \rangle \\ &+ \frac{1}{3} \mu \langle \nabla \cdot \mathbf{v}, \nabla \cdot \mathbf{u} \rangle - \langle \nabla \cdot \mathbf{v}, p \rangle \\ &+ \left\langle \frac{1}{c^2} q, \partial_t p \right\rangle + \left\langle \frac{1}{c^2} q, \mathbf{u} \cdot \nabla p \right\rangle + \langle \rho q, \nabla \cdot \mathbf{u} \rangle, \end{aligned} \tag{12}$$

$$\tilde{B}_{\mathrm{B}}([\mathbf{u}, p], \mathbf{v}) = - \langle \mathbf{v}, \mathbf{n} \cdot \sigma\left(\mathbf{u}, p\right) \rangle_\Gamma, \tag{13}$$

where the stress tensor is defined as $\sigma\left(\mathbf{u}, p\right) = -p\mathbf{I} + \mu \nabla \mathbf{u} + \frac{1}{3} \mu \left(\nabla \cdot \mathbf{u}\right) \mathbf{I}$. The Galerkin weak form of the problem prior to applying boundary conditions can be written as follows: for all time $t > 0$, find $\mathbf{u}(t) \in V$ and $p(t) \in Q$, with appropriate regularity in time, such that:

$$B([\mathbf{u}, p], [\mathbf{v}, \rho q]) + \tilde{B}_{\mathrm{B}}([\mathbf{u}, p], \mathbf{v}) = 0 \tag{14}$$

for all $\mathbf{v} \in V$ and $\rho q \in Q$. Moreover, initial conditions need to be appended. Boundary conditions will be defined in the following section, proposing a new formulation for the form $\tilde{B}_{\mathrm{B}}$. This will give rise to a decomposition of the form $\tilde{B}_{\mathrm{B}} = B_{\mathrm{B}} - L_{\mathrm{B}}$, with B_{B} depending on the unknowns and L_{B} on the boundary data, so that it can be moved to the right-hand-side of (14).

3. Imposition of boundary conditions

3.1. Mean and acoustic components

Although the intricate prescription of boundary conditions of the fully compressible formulation is avoided in the present problem, new challenges arise which need to be accounted for. Given that flow and acoustic scales need to be resolved together, an appropriate boundary condition for the acoustic component of the pressure must be used. The main objective of this boundary condition is to avoid the sound waves being backscattered by the external boundaries into the computational domain. There are several numerical methods which deal with this problem, see for instance the reviews in [27] and [28]. Here we highlight some of the most relevant ones. In [29] a non-reflecting boundary condition (NRBC) was presented for the Euler equations in multi-dimensional domains, modeling the waves using the characteristic equations. However, the identification of waves is not so straightforward in the Navier–Stokes equations and the assumption of one-dimensional flow on the boundaries had to be made [30]. This method yields proper results in boundaries where the solution is homogeneous

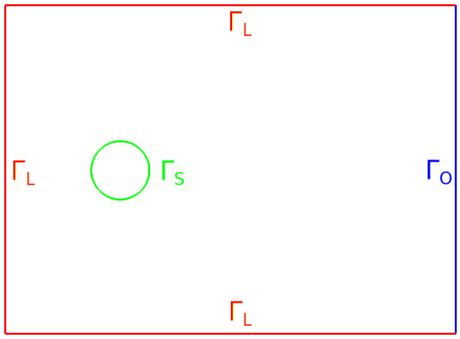

Fig. 1. Schematic definition of domain boundaries.

and known, such as the inlet. In [31], [32] and [33] the method was extended using low Mach number asymptotics in order to account for viscous and transverse effects on the wave. Another family of methods are the so called Perfectly Matched Layer (PML) methods, see [34] and [35], which can work under near-field conditions and thus allow for smaller computational domains to be used. These methods use an auxiliary domain beyond the outer boundaries which absorbs the incident waves without reflecting them back. A third alternative for the non-reflection of waves is the use of radiative and outflow conditions developed in [36] and extended in [37]. Similarly to the PML method, these works also consider a secondary domain, but in this case a modified set of equations minimizing reflection is solved at the far-field.

The treatment of the waves must be compatible with the flow velocity boundary conditions. This is of most importance on Dirichlet boundaries where the velocity needs to be prescribed. This need has motivated the development of a method for a unified prescription of flow and non-reflecting boundary conditions, which will be presented next. The method is able to deal with subsonic flows solved in arbitrary geometries, and following the aim of being a general formulation, it is compatible with any non-reflecting model for the acoustic waves, which will not be part of the work scope. The development of the method starts by splitting the two fields of the problem into mean variables $\bar{\mathbf{u}}$ and $\bar{p}$, and oscillatory components $\mathbf{u}'$ and p', as follows:

$$\begin{aligned} \mathbf{u}(\mathbf{x},t) &= \bar{\mathbf{u}}(\mathbf{x},t) + \mathbf{u}'(\mathbf{x},t), \\ p(\mathbf{x},t) &= \bar{p}(\mathbf{x},t) + p'(\mathbf{x},t), \end{aligned} \tag{15}$$

where

$$\begin{aligned} \bar{\mathbf{u}}(\mathbf{x},t) &:= \frac{1}{T_w}\int_{t-T_w}^{t} \mathbf{u}(\mathbf{x},s)\,ds \\ \bar{p}(\mathbf{x},t) &:= \frac{1}{T_w}\int_{t-T_w}^{t} p(\mathbf{x},s)\,ds \end{aligned} \tag{16}$$

and T_w is an appropriate time window. The mean flow variables are allowed to evolve during the calculation and they do not necessary need to be homogeneous along the boundary, but high frequency variations of these variables are not allowed because they would interfere with $[\mathbf{u}', p']$, which can be identified as the acoustic fluctuations. In other words, eq. (16) acts as a low pass filter that attenuates signals beyond a certain cutoff frequency that is determined by T_w.

3.2. Split boundary conditions

In order to treat flow and acoustic boundary conditions in an appropriate way, the boundary Γ has been divided into three disjoint subsets Γ_S, Γ_L and Γ_O, which will refer to the solid boundaries where velocity is prescribed to zero, the lateral walls and the outflow, respectively. Whereas the first and the latter ones have a clear physical meaning, Γ_L is defined for numerical convenience: it is composed of any outer boundary with at least one component of the velocity prescribed to a known value, which means that it also encompasses the inlet boundaries, see Fig. 1. The upper and lower walls belong to Γ_L because they have been assumed to be a mere truncation of the computational domain. This artificial truncation of the domain, which is performed with the objective of limiting the computational cost, does not assume that the affected boundaries are part of the outflow because this may not properly represent the physics of the flow and could even lead to numerical instabilities. Therefore, the flow needs to be confined without affecting the outward propagation of the waves. This boundary definition has been used for the two cases presented in Section 5.

On Γ_L and Γ_O, the far-field conditions assume that the acoustic scales are dominant. This means that a naive approach using a zero traction boundary condition would lead to reflection of the waves into the domain. Therefore, a non-reflecting numerical model must be applied on these boundaries, see for example [21].

The proposed methodology for applying compatible flow and acoustic boundary conditions on Γ_L and Γ_O is based on a weak or weighted prescription of the Dirichlet conditions together with the use of a Sommerfeld type boundary condition. The boundary conditions for the problem can be formulated as described next.

On the solid boundary Γ_S, where the velocity is known and the incident waves are expected to reflect, we enforce:

$$\mathbf{u} = \bar{\mathbf{u}} + \mathbf{u}' = \mathbf{u}_S \text{ on } \Gamma_S,$$

where $\mathbf{u}_S$ is the prescribed velocity on the solid boundary.

On the truncation boundary Γ_L, several conditions are going to be enforced: firstly, the mean value of the velocity is going to be prescribed to the inlet (or truncation) boundary velocity $\mathbf{u}_L$:

$$\bar{\mathbf{u}} = \mathbf{u}_L \quad \text{on } \Gamma_L.$$

Secondly, a Sommerfeld-like boundary condition for the fluctuating part of the velocity and pressure fields is prescribed:

$$\mathbf{n} \cdot \mathbf{u}' = -\frac{1}{\rho c}\mathbf{n} \cdot \left[\mathbf{n} \cdot \sigma\left(\mathbf{u}', p'\right)\right] \quad \text{on } \Gamma_L,$$

where $\mathbf{n}$ is the unit outward normal to Γ_L. Let also $\mathbf{m}$ be any unit vector tangent to it. The fluctuating tractions in the tangential direction are prescribed to zero:

$$\mathbf{m} \cdot \left[\mathbf{n} \cdot \sigma\left(\mathbf{u}', p'\right)\right] = 0 \text{ on } \Gamma_L.$$

Finally, on the outflow boundary Γ_O, the following conditions are going to be applied:

$$\mathbf{n} \cdot \sigma\left(\bar{\mathbf{u}}, \bar{p}\right) = \mathbf{t}_O \quad \text{on } \Gamma_O,$$

which enforces the mean value tractions to the prescribed value $\mathbf{t}_O$. Regarding the fluctuating values, the same approach used for Γ_L is used, now with a Sommerfeld-like condition in the normal direction and zero traction prescribed in the tangential directions:

$$\begin{aligned} \mathbf{n} \cdot \mathbf{u}' &= -\frac{1}{\rho c}\mathbf{n} \cdot \left[\mathbf{n} \cdot \sigma\left(\mathbf{u}', p'\right)\right] && \text{on } \Gamma_O, \\ \mathbf{m} \cdot \left[\mathbf{n} \cdot \sigma\left(\mathbf{u}', p'\right)\right] &= 0 && \text{on } \Gamma_O. \end{aligned}$$

Note that:

- Γ_S is a classical Dirichlet-type boundary. Velocity test functions will vanish there and the condition $\mathbf{u} = \mathbf{u}_S$ can be prescribed in a strong way.
- Γ_L is a boundary where Dirichlet-type boundary conditions are prescribed for $\bar{\mathbf{u}}$ and mixed boundary conditions for $\mathbf{u}'$, namely the normal component and the tangent associated stress. Both will be prescribed weakly.
- Γ_O is a boundary where Neumann-type boundary conditions are prescribed for $\bar{\mathbf{u}}$ and mixed boundary conditions for $\mathbf{u}'$, the same as on Γ_L. All these conditions will be prescribed weakly.
- For inviscid flows, the condition on the normal component of $\mathbf{u}'$ reduces to Sommerfeld's condition $p' = \rho c\left(\mathbf{u}' \cdot \mathbf{n}\right)$. Obviously, other non-reflecting boundary conditions could be used.

Let us see how to prescribe these boundary conditions in the variational form of the problem. Let us start by noting that

$$\begin{aligned} -\langle \mathbf{v}, \mathbf{n} \cdot \sigma(\mathbf{u}, p)\rangle_\Gamma &= -\langle \mathbf{v}, \mathbf{n} \cdot \sigma(\mathbf{u}, p)\rangle_{\Gamma_L} - \langle \mathbf{v}, \mathbf{n} \cdot \sigma(\mathbf{u}, p)\rangle_{\Gamma_O} \\ &= -\langle \mathbf{v}, \mathbf{n} \cdot \sigma(\bar{\mathbf{u}}, \bar{p})\rangle_{\Gamma_L} - \langle \mathbf{v}, \mathbf{n} \cdot \sigma\left(\mathbf{u}', p'\right)\rangle_{\Gamma_L} \\ &\quad - \langle \mathbf{v}, \mathbf{n} \cdot \sigma(\bar{\mathbf{u}}, \bar{p})\rangle_{\Gamma_O} - \langle \mathbf{v}, \mathbf{n} \cdot \sigma\left(\mathbf{u}', p'\right)\rangle_{\Gamma_O} \\ &= -\langle \mathbf{v}, \mathbf{n} \cdot \sigma(\bar{\mathbf{u}}, \bar{p})\rangle_{\Gamma_L} + \langle \rho c \mathbf{v} \cdot \mathbf{n}, \mathbf{u}' \cdot \mathbf{n}\rangle_{\Gamma_L} \\ &\quad - \langle \mathbf{v}, \mathbf{t}_O\rangle_{\Gamma_O} + \langle \rho c \mathbf{v} \cdot \mathbf{n}, \mathbf{u}' \cdot \mathbf{n}\rangle_{\Gamma_O}. \end{aligned} \tag{17}$$

Note that no contribution on Γ_S has been included, since in this boundary usual Dirichlet boundary conditions are applied and the test functions vanish on it. We still need to prescribe $\bar{\mathbf{u}} = \mathbf{u}_L$, which will be done through penalization using Nitsche's method [38]. In the spirit of this method, it is convenient to symmetrize the boundary terms. Taking this into account we define the boundary terms, which can be written as $B_B([\mathbf{u}, p], [\mathbf{v}, q]) - L_B([\mathbf{v}, q])$, with

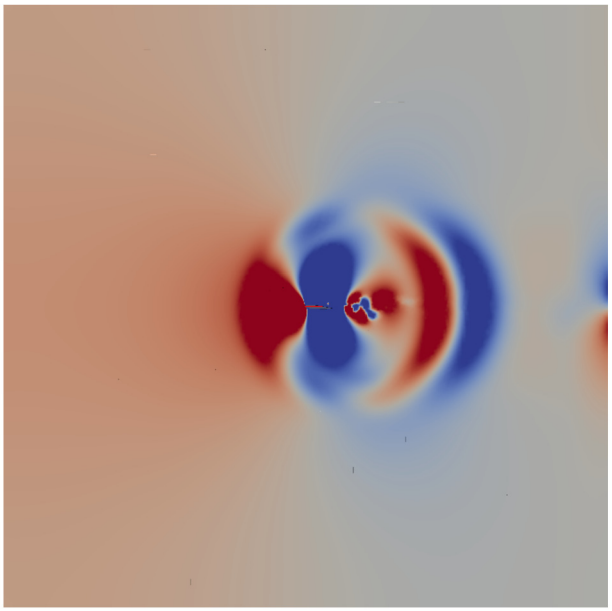

Fig. 2. Reflection of the sound generated by vortices approaching the outflow.

$$
\begin{aligned}
B_{\mathrm{B}}([\mathbf{u}, p], [\mathbf{v}, q]) := & -\langle \mathbf{v}, \mathbf{n} \cdot \sigma\left(\bar{\mathbf{u}}, \bar{p}\right)\rangle_{\Gamma_L} - \langle \bar{\mathbf{u}}, \mathbf{n} \cdot \sigma\left(\mathbf{v}, q\right)\rangle_{\Gamma_L} + \beta \frac{\mu_p}{l_p} \langle \mathbf{v}, \bar{\mathbf{u}}\rangle_{\Gamma_L} \\
& + \langle \rho c \mathbf{v} \cdot \mathbf{n}, \mathbf{u}' \cdot \mathbf{n}\rangle_{\Gamma_L} + \langle \rho c \mathbf{v} \cdot \mathbf{n}, \mathbf{u}' \cdot \mathbf{n}\rangle_{\Gamma_O}, \\
L_{\mathrm{B}}([\mathbf{v}, q]) := & -\langle \mathbf{u}_L, \mathbf{n} \cdot \sigma\left(\mathbf{v}, q\right)\rangle_{\Gamma_L} + \beta \frac{\mu_p}{l_p} \langle \mathbf{v}, \mathbf{u}_L\rangle_{\Gamma_L} + \langle \mathbf{v}, \mathbf{t}_O\rangle_{\Gamma_O},
\end{aligned}
\tag{18}
$$

where β, μ_p, l_p are numerical parameters, the first one dimensionless, the second one with units of viscosity and the latter with units of length. We are still at the continuous level. When a finite element approximation in space is performed, h being the element size, one can show that μ_p, l_p can be taken as $\mu_p = \mu + |\mathbf{u}|h$, and $l_p = h$ [39].

The only ingredient missing in the formulation is the definition of the outflow traction $\mathbf{t}_O$. Assuming that Γ_O is placed in a far-field region, where $\bar{p} \approx 0$ and $\nabla \bar{\mathbf{u}} \approx 0$, then the natural condition to be imposed is $\mathbf{t}_O = \mathbf{0}$.

3.3. Domain truncation

The truncation of the domain is a problematic issue when dealing with acoustic waves. Sometimes, especially in case of low speed flows, the far field conditions are reached within a small distance of the solid objects causing the perturbation. In these cases the truncation of the domain will only depend on the measure of the largest wavelength. Therefore, in such scenarios the present formulation can be applied in a general way without further artifacts. However, when convection becomes dominant stagnation conditions may be found far away from the perturbation, which results in a high computational cost if the full near-field domain needs to be simulated. Moreover, many times the Sommerfeld non-radiating boundary condition is compromised, since it assumes an orthogonal incidence of the wave with the external boundary.

An example illustrating this situation is depicted in Fig. 2. In this case a $\mathrm{M} = 0.4$ flow over a wing profile is calculated departing from a fully developed incompressible flow solution. Before any wave reaches the boundary, the outlet is already reflecting the noise produced by the vortices passing through it, see Fig. 2.

In the second numerical example shown in Section 5, this problem has been solved by adding a spherical PML based on [40] in an artificial outlet domain Ω_{PML}, see Fig. 3. For this, we define the finite element contribution of the PML layer in a new bilinear form B_{PML}:

$$
B_{\mathrm{PML}}([\mathbf{u}, p], [\mathbf{v}, q]) := (\mathbf{v}, \alpha^* \mathbf{u}) + (q, \rho \alpha p)
\tag{19}
$$

where α is defined as

$$
\begin{aligned}
\alpha(r) = 0.4 \frac{(r - r_0)^2}{\left(r_f - r_0\right)^3} \left(-2r + 3r_f - r_0\right) \quad & \text{in } \Omega_{\mathrm{PML}}, \\
\alpha(r) = 0 \quad & \text{in } \Omega \setminus \Omega_{\mathrm{PML}},
\end{aligned}
\tag{20}
$$

where $\alpha^* = \alpha \rho^2 c^2$ and r_0 and r_f are the small and big radius of the PML, respectively.

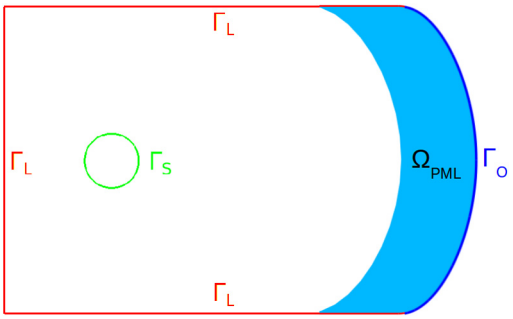

Fig. 3. A PML is attached to the original outlet of the domain Ω.

Taking the previous considerations into account, the final problem to be solved consists of finding $[\mathbf{u}, p]$ such that

$$B([\mathbf{u}, p], [\mathbf{v}, q]) + B_{\text{PML}}([\mathbf{u}, p], [\mathbf{v}, q]) + B_{\text{B}}([\mathbf{u}, p], [\mathbf{v}, q]) = L_{\text{B}}([\mathbf{v}, q]) \tag{21}$$

for all test functions $[\mathbf{v}, q]$.

Unlike in Section 3, the importance of absorbing both hydrodynamic and acoustic scales on the outlet justifies the application of the PML to the whole variables $[\mathbf{u}, p]$. The performance of this numerical tool will be presented in Section 5.

4. Numerical approximation

In this section we present the finite element formulation for the space approximation of the isentropic Navier–Stokes equations, including the stabilization terms required for obtaining a stable formulation when using equal velocity-pressure interpolations, in particular linear-linear (P_1/P_1) elements, as well as the time discretization using finite differences.

Let us consider a finite element partition of the domain Ω of size h, and use this letter as subscript to denote finite element functions and spaces. Only conforming finite element approximations will be considered in what follows. Let $V_h \subset V$ be the finite approximation space for the discrete velocity field and let us also define $Q_h \subset Q$, the pressure approximation space.

4.1. Time discretization

Concerning the time integration, the monolithic approach for solving the incompressible Navier–Stokes equations consists in building a system with both velocity and pressure degrees of freedom, which leads to the coupled calculation of the momentum and mass equations in one single step. To approximate the first order time derivatives, a second order backward finite difference scheme (BDF2) has been used. Let us partition the time interval $[0, T]$ into N equal time steps of size $\delta t := t^{n+1} - t^n$ so that $0 \equiv t^0 < t^1 < \ldots < t^n < \ldots < t^N \equiv T$. Given a generic time dependent function $g(t)$, the following notation will be used for the BDF2 approximation to the first time derivative:

$$\partial_t g|_{t^{n+1}} \approx \delta_t g^{n+1} := \frac{1}{\delta t}\left(\frac{3}{2}g^{n+1} - 2g^n + \frac{1}{2}g^{n-1}\right), \tag{22}$$

where g^n denotes the evaluation of g at time step t^n.

Obviously other time integration schemes could be used, both implicit and explicit. The latter would require mass lumping to avoid the solution of linear systems using a finite element approximation (see below); this is easy only for linear elements. Moreover, implicit time integration allows reaching the incompressible limit. We therefore favor the use of implicit integrators, as BDF2.

4.2. Discrete boundary conditions

At an arbitrary time step of the numerical simulation, the final fully discretized implicit scheme in space and time can be derived using the finite element formulation described below. Moreover, the mean flow values must be expressed according to the chosen integration scheme and the penalty parameters of the weak essential condition on Γ_L must be defined. We do this as follows:

- As mentioned above, μ_p, l_p can be taken as $\mu_p = \mu + |\mathbf{u}|h$, $l_p = h$ [39].
- If the temporal window presented at Eq. (16) is defined at a discrete level as $T_w = N_w \delta t$ and we use the trapezoidal rule for the integration, then the mean values can be expressed as follows:

$$\bar{\mathbf{u}}_h^{n+1} = \frac{\delta t}{T_w}\left(\frac{1}{2}\mathbf{u}_h^{n+1} + \sum_{k=n-N_w+2}^{n}\mathbf{u}_h^k + \frac{1}{2}\mathbf{u}_h^{n-N_w+1}\right). \tag{23}$$

This expression of the mean flow values keeps the temporal integration implicit and second order accurate. Bearing in mind the (usually) sharp initial pressure transient and the absence of a minimally developed mean flow, it is important to run several time steps (N_w) before using the present formulation in order to obtain representative mean flow variables. The same procedure is applied to p and the fluctuating components will be also expressed from now on in terms of the full variables evaluated at t^{n+1}. The trapezoidal rule in eq. (23) can be viewed as a particular realization of a causal finite impulse response (FIR) filter of order $N_w + 1$. By modifying the coefficients that multiply the discrete velocities, one could design a time scheme that filters the frequencies higher than a given cutoff value.

4.3. Finite element approximation

For clarity, the formulation will be arranged in five forms: B, B_{B}, B_{PML}, L_{B} and B_{S}; the latter corresponds to the stabilization terms and will be presented next. The final formulation reads as follows: from known $\mathbf{u}_h^{n-2}$, $\mathbf{u}_h^{n-1}$ and $\mathbf{u}_h^n$, compute the compressible velocity and pressure at time step t^{n+1}, $\left[\mathbf{u}_h^{n+1}, p_h^{n+1}\right] \in V_h \times Q_h$, such that

$$\begin{aligned} &B^{n+1}([\mathbf{u}_h, p_h], [\mathbf{v}_h, q_h]) + B_{\mathrm{PML}}^{n+1}([\mathbf{u}_h, p_h], [\mathbf{v}_h, q_h]) + B_{\mathrm{B}}^{n+1}([\mathbf{u}_h, p_h], [\mathbf{v}_h, q_h]) \\ &\quad + B_{\mathrm{S}}^{n+1}([\mathbf{u}_h, p_h], [\mathbf{v}_h, q_h]) = L_{\mathrm{B}}^{n+1}([\mathbf{v}_h, q_h]), \end{aligned} \tag{24}$$

for all test functions, where

$$\begin{aligned} B^{n+1}([\mathbf{u}_h, p_h], [\mathbf{v}_h, q_h]) = &\left\langle \rho^{n+1}\mathbf{v}_h, \delta_t \mathbf{u}_h^{n+1}\right\rangle + \langle \rho^{n+1}\mathbf{v}_h, \left(\mathbf{u}_h^{n+1}\cdot\nabla\right)\mathbf{u}_h^{n+1}\rangle \\ &+ \mu\left\langle \nabla\mathbf{v}_h, \nabla\mathbf{u}_h^{n+1}\right\rangle + \frac{1}{3}\mu\left\langle \nabla\cdot\mathbf{v}_h, \nabla\cdot\mathbf{u}_h^{n+1}\right\rangle \\ &- \left\langle \nabla\cdot\mathbf{v}_h, p_h^{n+1}\right\rangle + \left\langle \frac{1}{\left(c^2\right)^{n+1}} q_h, \delta_t p_h^{n+1}\right\rangle \\ &+ \left\langle \frac{1}{\left(c^2\right)^{n+1}} q_h, \mathbf{u}_h^{n+1}\cdot\nabla p_h^{n+1}\right\rangle + \left\langle \rho^{n+1} q_h, \nabla\cdot\mathbf{u}_h^{n+1}\right\rangle. \end{aligned} \tag{25}$$

Note that this expression involves both the unknowns at time step $n+1$ and at previous time steps. For the rest of the terms in (24), the superscript $n+1$ indicates that both the unknowns and the data are evaluated at time step $n+1$.

As mentioned before, the condensation of ρ^{n+1} and c^{n+1} is essential for keeping the complexity of the formulation low. They are evaluated with the converged unknowns of the problem at t^{n+1}, as the implicit scheme requires:

$$\begin{aligned} \rho^{n+1} &= \rho_0\left(1 + \frac{\gamma-1}{2}\frac{|\mathbf{u}_h^{n+1}|^2}{c_0^2}\right)^{\gamma-1}, \\ \left(c^2\right)^{n+1} &= c_0^2\left(1 + \frac{\gamma-1}{2}\frac{|\mathbf{u}_h^{n+1}|^2}{c_0^2}\right)^{-1}. \end{aligned} \tag{26}$$

We have included the evaluation of ρ^{n+1} and c^{n+1} in the non-linearity loop in a fixed point manner, that is say, when computing the unknowns at a certain iteration we use the values of ρ^{n+1} and c^{n+1} at the previous one, and once the unknowns are computed we update them. Note that they are required at the integration points within each finite element domain. To simplify the notation, since it is understood that ρ and c are only evaluated at t^{n+1}, from now on they will be referred as ρ and c instead of ρ^{n+1} and c^{n+1}.

Next, the bilinear form B_{B}^{n+1} and the linear form L_{B}^{n+1} can be easily obtained using (18):

$$\begin{aligned} B_{\mathrm{B}}^{n+1}([\mathbf{u}_h, p_h], [\mathbf{v}_h, q_h]) = &-\langle \mathbf{v}_h, \mathbf{n}\cdot\sigma_h\left(\bar{\mathbf{u}}_h^{n+1}, \bar{p}_h^{n+1}\right)\rangle_{\Gamma_L} \\ &- \langle \bar{\mathbf{u}}_h^{n+1}, \mathbf{n}\cdot\sigma_h\left(\mathbf{v}_h, q_h\right)\rangle_{\Gamma_L} + \beta\frac{\mu_p}{l_p}\langle \mathbf{v}_h, \bar{\mathbf{u}}_h^{n+1}\rangle_{\Gamma_L} + \langle \rho c\mathbf{v}_h\cdot\mathbf{n}, \mathbf{u}_h'^{n+1}\cdot\mathbf{n}\rangle_{\Gamma_L\cup\Gamma_O}, \\ L_{\mathrm{B}}^{n+1}([\mathbf{v}_h, q_h]) = &\beta\frac{\mu_p}{l_p}\langle \mathbf{v}_h, \mathbf{u}_L^{n+1}\rangle_{\Gamma_L} - \langle \mathbf{u}_L^{n+1}, \mathbf{n}\cdot\sigma_h\left(\mathbf{v}_h, q_h\right)\rangle_{\Gamma_L}, \end{aligned}$$

where we have assumed that $\mathbf{t}_O = \mathbf{0}$. Applying the definition of the mean values presented in Eq. (23) and expressing the fluctuating components in terms of the problem unknowns, B_{B}^{n+1} can be rewritten as follows:

$$
\begin{aligned}
B_{\mathrm{B}}^{n+1}([\mathbf{u}_h, p_h], [\mathbf{v}_h, q_h]) &= -\frac{1}{2N_w}\langle \mathbf{v}_h, \mathbf{n}\cdot\sigma_h\left(\mathbf{u}_h^{n+1}, p_h^{n+1}\right)\rangle_{\Gamma_L} \\
&- \frac{1}{2N_w}\langle \mathbf{u}_h^{n+1}, \mathbf{n}\cdot\sigma_h\left(\mathbf{v}_h, q_h\right)\rangle_{\Gamma_L} + \left(1-\frac{1}{2N_w}\right)\langle \rho c\mathbf{v}_h\cdot\mathbf{n}, \mathbf{u}_h^{n+1}\cdot\mathbf{n}\rangle_{\Gamma_L\cup\Gamma_O} \\
&+ \frac{\beta}{2N_w}\frac{\mu_p}{l_p}\langle \mathbf{v}_h, \mathbf{u}_h^{n+1}\rangle_{\Gamma_L} + \frac{\beta}{N_w}\frac{\mu_p}{l_p}\Big[\sum_{k=n-N_w+2}^{n}\langle \mathbf{v}_h, \mathbf{u}_h^{k}\rangle_{\Gamma_L} - \frac{1}{2}\langle \mathbf{v}_h, \mathbf{u}_h^{n-N_w+1}\rangle_{\Gamma_L}\Big] \\
&- \frac{1}{N_w}\sum_{k=n-N_w+2}^{n}\langle \mathbf{v}_h, \mathbf{n}\cdot\sigma_h\left(\mathbf{u}_h^{k}, p_h^{k}\right)\rangle_{\Gamma_L} \\
&+ \frac{1}{2N_w}\langle \mathbf{v}_h, \mathbf{n}\cdot\sigma_h\left(\mathbf{u}_h^{n-N_w+1}, p_h^{n-N_w+1}\right)\rangle_{\Gamma_L} \\
&- \frac{1}{N_w}\Big[\sum_{k=n-N_w+2}^{n}\langle \mathbf{u}_h^{k}, \mathbf{n}\cdot\sigma_h\left(\mathbf{v}_h, q_h\right)\rangle_{\Gamma_L} - \frac{1}{2}\langle \mathbf{u}_h^{n-N_w+1}, \mathbf{n}\cdot\sigma_h\left(\mathbf{v}_h, q_h\right)\rangle_{\Gamma_L}\Big] \\
&- \frac{1}{N_w}\sum_{k=n-N_w+2}^{n}\langle \rho c\mathbf{v}_h\cdot\mathbf{n}, \mathbf{u}_h^{k}\cdot\mathbf{n}\rangle_{\Gamma_L\cup\Gamma_O} - \frac{1}{2N_w}\langle \rho c\mathbf{v}_h\cdot\mathbf{n}, \mathbf{u}_h^{n-N_w+1}\cdot\mathbf{n}\rangle_{\Gamma_L\cup\Gamma_O}. \\
L_{\mathrm{B}}^{n+1}([\mathbf{v}_h, q_h]) &= \beta\frac{\mu_p}{l_p}\langle \mathbf{v}_h, \mathbf{u}_L^{n+1}\rangle_{\Gamma_L} - \langle \mathbf{u}_L^{n+1}, \mathbf{n}\cdot\sigma_h\left(\mathbf{v}_h, q_h\right)\rangle_{\Gamma_L}.
\end{aligned}
$$

Note that several terms of B_{B}^{n+1} can be computed with values of velocities and pressure of previous time steps, and therefore moved to the right-hand-side in the final equation.

When a PML is mandatory, B_{PML}^{n+1} must be included in the formulation. Using (19) the discrete bilinear form for the PML can be easily derived:

$$
B_{\mathrm{PML}}^{n+1}([\mathbf{u}_h, p_h], [\mathbf{v}_h, q_h]) = \alpha^*\left(\mathbf{v}_h, \mathbf{u}_h^{n+1}\right)_{\Omega_{\mathrm{PML}}} + \alpha\left(q_h, \rho p_h^{n+1}\right)_{\Omega_{\mathrm{PML}}}. \tag{27}
$$

The last ingredient for a robust and consistent formulation consists in applying an appropriate stabilization for the convective terms and for the fulfillment of the velocity-pressure inf-sup condition [41], since equal interpolation elements are being used. In the present case, the Algebraic Subgrid Scale (ASGS) method for incompressible flows presented in [42] has been taken as reference and extended to isentropic flows. This is the simplest version of Variational Multiscale (VMS) finite element methods (see [43] for a review). The only care that needs to be taken when designing the stabilization terms is that the continuity equation now has two more additional terms compared to the case of incompressible flows that need to be taken into account, both in the residual of this equation and in the operator applied to the test functions that multiplies this residual. The final result is:

$$
\begin{aligned}
&B_{\mathrm{S}}^{n+1}\left([\mathbf{u}_h, p_h], [\mathbf{v}_h, q_h]\right) \\
&\quad= \sum_K \tau_{1,K}\big\langle \rho\mathbf{u}_h^{n+1}\cdot\nabla\mathbf{v}_h + \nabla q_h, \rho\delta_t\mathbf{u}_h^{n+1} + \rho\mathbf{u}_h^{n+1}\cdot\nabla\mathbf{u}_h^{n+1} - \nabla\cdot\sigma_h^{n+1}\big\rangle_K \\
&\quad+ \sum_K \tau_{2,K}\big\langle \rho\nabla\cdot\mathbf{v}_h + \frac{1}{c^2}\mathbf{u}_h^{n+1}\cdot\nabla q_h, \\
&\qquad\rho\nabla\cdot\mathbf{u}_h^{n+1} + \frac{1}{c^2}\mathbf{u}_h^{n+1}\cdot\nabla p_h^{n+1} + \frac{1}{c^2}\delta_t p_h^{n+1}\big\rangle_K,
\end{aligned}
\tag{28}
$$

where K denotes a generic element domain, summation is done over all elements of the finite element mesh, and $\tau_{1,K}$ and $\tau_{2,K}$ are suitable stabilization parameters defined in each element [44], that we compute as:

$$
\tau_{1,K} = \left[c_1\frac{\mu}{h^2} + c_2\rho\frac{|\mathbf{u}_h^{n+1}|_K}{h}\right]^{-1}, \qquad \tau_{2,K} = \frac{h^2}{c_1\tau_{1,K}},
$$

$|\mathbf{u}_h^{n+1}|_K$ being the mean Euclidean norm of the velocity in element K. The algorithmic constants c_1 and c_2 depend on the polynomial order of the interpolation. We set them to $c_1 = 4$ and $c_2 = 2$ for linear elements. Note that in (28) we have not considered operator associated to the stresses applied to the test functions multiplying the residual of the momentum equation. Likewise, in order to keep the presentation concise we have not considered neither time dependent subscales [45], nor orthogonal subgrid scales [44], although we favor these two options.

Table 1
Vortex shedding frequency (Hz) at three different points.

Solver/Point	1	2	3
Incompressible	15.601	15.723	15.898
Isentropic compressible	15.576	15.601	15.625
Fully compressible	15.775	15.779	15.855

5. Results

For a proper validation of the present formulation three different scenarios have been taken as reference. First, a 2D problem consisting in a low speed $\mathrm{Re} = 1000$ flow around a cylinder has been calculated with the isentropic compressible equations for comparing the CFD results and the acoustic propagation to those provided by an incompressible solver and the Lighthill analogy [46], and to those obtained when using a compressible flow formulation with primitive variables presented in [47]. Second, a $\mathrm{M} = 0.4$ flow around a 3D NACA 0012 airfoil has been calculated in order to evaluate the performance of the formulation against a compressible flow solver and the Ffowcs Williams & Hawkings (FWH) acoustic analogy. Finally, a 2D $\mathrm{M} = 0.7$ flow past an open cavity has been simulated for a quantitative validation of the solver in cases of acoustic feedback to the flow. The main advantage of the isentropic compressible formulation is that it can be treated numerically like the incompressible formulation, although the flow regime might not be in the incompressible range anymore. From the point of view of an end user, the only further requirement consists in introducing the four following parameters: the gas universal constant $R = 8.31$ J/K·mol, the molar mass, the sound propagation speed of the working gas and the bulk temperature. In both cases the values of air at room temperature have been considered ($\mathcal{M} = 28.97$ g/mol, $c_0 = 343$ m/s and $T_0 = 293.15$ K).

5.1. Aerodynamic sound radiated by flow past a cylinder. $M = 0.0583$

The first benchmark case consists in a 2D flow around a cylinder of diameter $D = 0.3$, which allows evaluating the aeolian tones of a low Mach viscous flow [46]. The incident velocity of 20 leads to a Reynolds and Mach numbers at the far field (away from the cylinder) of $\mathrm{Re} = 1000$ and $\mathrm{M} = 0.0583$ for a sound speed of $c_0 = 343$ (all units are in SI). The problem has been solved in an unstructured mesh of nearly 1 million triangular linear elements using equal interpolation for velocity and pressure, with a size of $3 \times 10^{-3} D$ near the cylinder surface. The case has been run up to 1.5 s with a time step $\delta t = 1 \times 10^{-3}$ s, departing from an initial incompressible solution in order to ease the initial convergence of the iterative solver. For the weak imposition of boundary conditions it has been enough taking a penalty parameter $\beta = 1$.

The original case in [46] was computed with the incompressible Navier–Stokes equations and Lighthill's analogy, which is a realistic approach for this flow range. However, one of the main goals of this work consists in showing that, given a low Mach number and a fine enough discretization, the present formulation converges to the solution of a Direct Numerical Simulation. For this reason, the case has been also computed with the formulation in [47], which despite a high computational cost manages to overcome the poor performance of compressible conservative schemes in the incompressible range.

Regarding the flow solution, the first result to be analyzed is the vortex shedding frequency and the dispersive error of the wave propagation along the domain. In order to filter the main frequency mode from the noise produced by secondary vortices, three points located on the perpendicular direction to the flow have been selected. Point 1 is located just below the cylinder, point 3 lays near the lower boundary of the domain and point 2 in the middle between 1 and 3. Table 1 presents the vortex shedding frequency computed with the pressure time history for all three formulations at the three chosen locations. The obtained ranges of values show that, in spite of being near the incompressible limit and using the same spatial discretization and the same temporal integrator, the dispersive error of the isentropic approximation is similar to that of the fully compressible solver and much smaller than the incompressible one.

The fully developed velocity profiles are compared in Fig. 4. This very good fitting between all three velocity profiles shows the possibility of replacing the incompressible solvers when their convergence is not satisfactory even if the acoustics are not relevant, as well as the fully compressible formulation when dealing with low speed flows. Moreover, it confirms the good performance of the weakly imposed inlet condition. Of course, one may think that, despite this benefit, the compressibility brings the big drawback of waves being reflected by the boundaries and polluting the flow solution. However, Fig. 5 shows that this inconvenience is completely resolved by the previously presented boundary conditions as no reflections are observed on the external boundaries. This plot also validates qualitatively the acoustic propagation at the far field. The present formulation is capable of capturing the anisotropy of the aeolian tones as well as the amplitude of the acoustic waves. On the other hand, Fig. 6 aims for a quantitative validation of the phenomenon. In this sense, the wave propagation obtained with the isentropic compressible solver reproduces with small error the solution of both incompressible and fully compressible formulations, from which we can conclude that the method converges to a DNC at the low Mach range.

A very important issue which has been already highlighted in the Introduction is the computational cost of the formulation in comparison to the state-of-the-art incompressible and fully compressible approaches using primitive variables. Table 2 shows the number of non-linearity iterations and the cost per iteration using a Biconjugate Gradients linear solver without any preconditioning. This non-optimized configuration has been chosen because it has yielded convergence for all

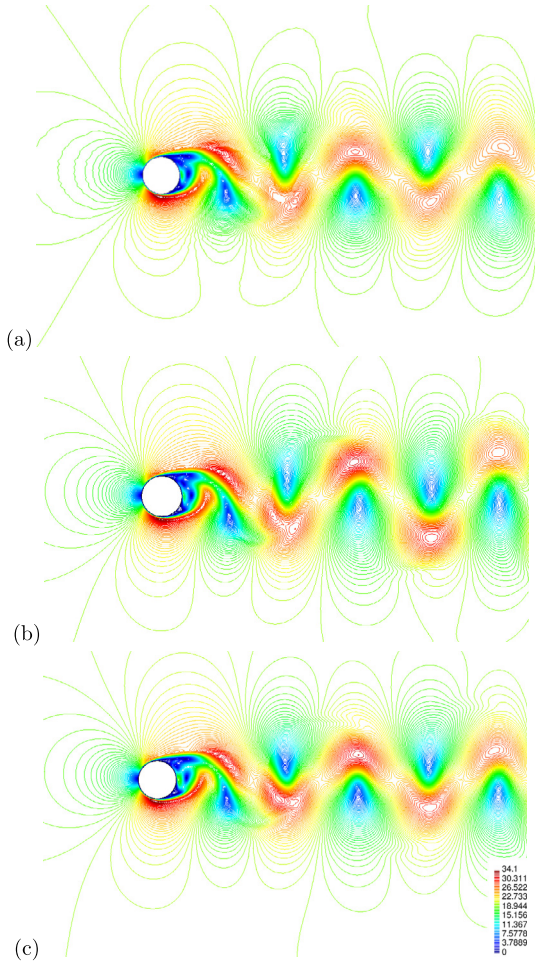

Fig. 4. DNS compressible flow velocity (a), incompressible flow velocity (b), isentropic compressible flow velocity (c). (For interpretation of the colors in the figure(s), the reader is referred to the web version of this article.)

three formulations. The results reveal the poor performance of monolithic incompressible schemes in problems of this size ($\sim 360,000$ elements) due to the divergence-free condition, as well as a huge cost saving respect to the fully compressible approach, which has needed a ten times smaller time step for reaching convergence.

5.2. *Aerodynamic sound radiated by flow past an airfoil.* $M = 0.4$

The second benchmark case consists in a 3D flow around a NACA 0012 airfoil with an angle of attack of 5° [48], which will be used for a general qualitative validation of the present formulation for large-sized problems involving high-speed subsonic flows. The flow Reynolds number based on the airfoil chord ($d = 0.1524$) is $\mathrm{Re}_c = 408,000$, whereas the incident Mach number is $\mathrm{M} = 0.4$. The problem has been solved in an unstructured mesh of nearly 20 million tetrahedral linear elements using equal interpolation for velocity and pressure, with a size of 4×10^{-4} on the leading edge and 6.5×10^{-4} on the rest of the airfoil surface (all units are in SI). The case has been run up to 0.050 s with a time step $\delta t = 10^{-5}$ s, departing from an initial incompressible solution in order to ease the initial convergence of the iterative solver. For the weak imposition of boundary conditions a penalty parameter $\beta = 125$ has been taken. Unlike the previous low-speed flow, the present case generates an airjet that cannot be dissipated before reaching the outlet, for which a PML has been placed in this region. On the external boundaries the flow field has been prescribed separately following the method presented in Section 3.

The original case in [48] was computed with a compressible Large Eddy Simulation (LES) for the flow scales and the Ffowcs Williams & Hawkings (FWH) acoustic analogy for the acoustic component [9]. Since the object of the present work does not consist in assessing the performance of the solver in specific mesh typologies or in reproducing all the details of a particular problem, but in establishing a general framework for the calculation of a wide range of flows, the goal of this analysis has been restricted to the following points: the suitability of the present isentropic compressible formulation

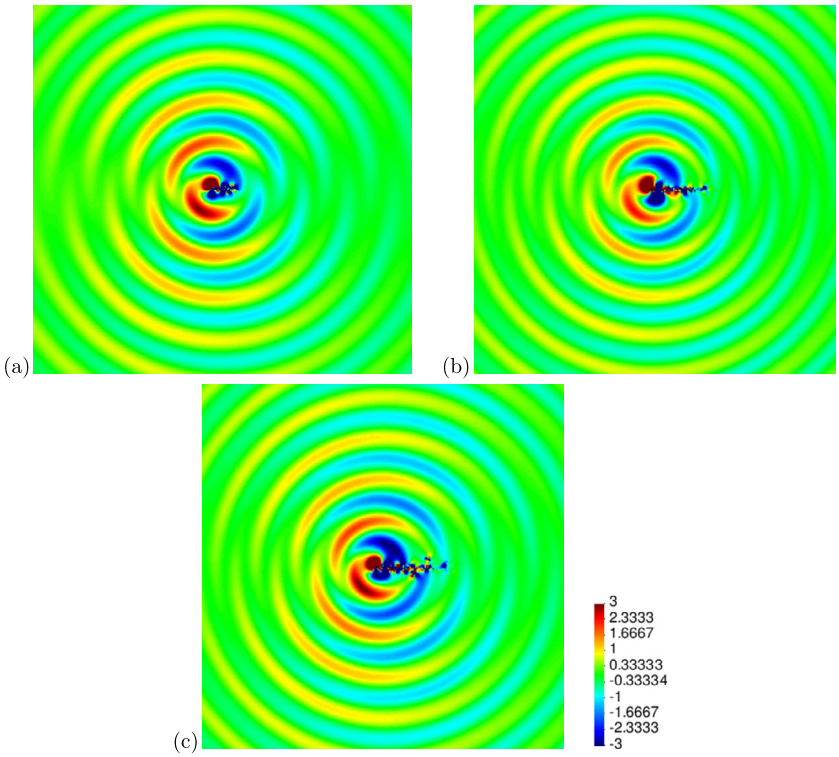

Fig. 5. DNS compressible flow pressure (a), acoustic pressure calculated with the incompressible Lighthill analogy (b), isentropic compressible flow pressure (c).

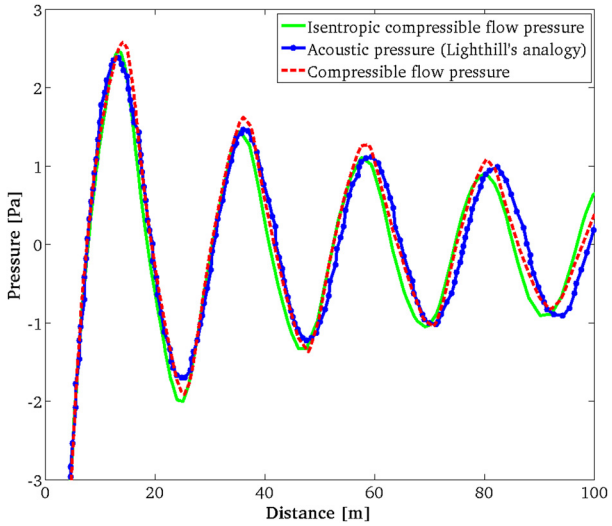

Fig. 6. Wave propagation at 90° with respect to the x-axis.

Table 2
Computational cost for all three formulations using the same linear solver and no preconditioner.

Solver	# Picard iterations	Cost/iteration (s)
Incompressible	10	65.0
Isentropic compressible	4	2.3
Fully compressible	4	3.8

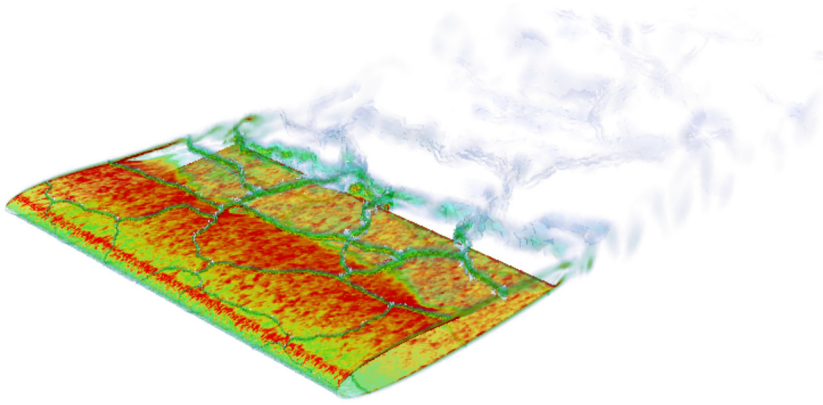

Fig. 7. Vorticity profile on the airfoil.

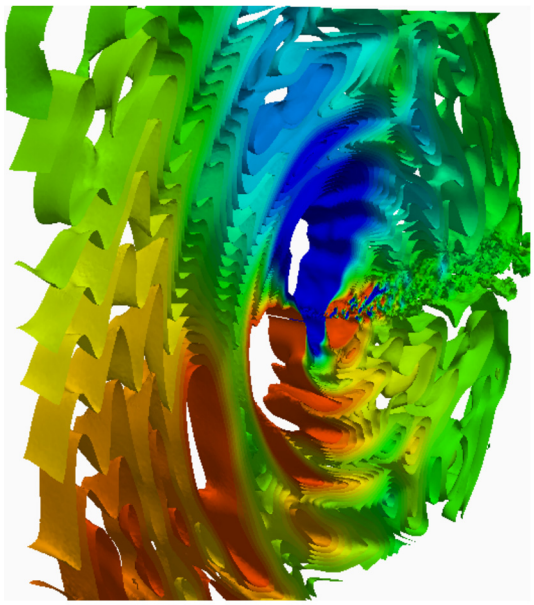

Fig. 8. Pressure isosurfaces.

for reproducing the mean flow patterns at $M = 0.4$, the proper propagation of the captured acoustic modes, and finally the validation of the proposed boundary conditions.

Figs. 7 and 8 show the calculated vorticity profile on the airfoil and the pressure isosurfaces with the corresponding wave propagation, respectively. Due to the highly aerodynamic character of this profile, the validation of the formulation in regard to the mean flow variables is very dependent to a proper description of the boundary layer. A wall-law with both buffer and logarithmic regions has been prescribed on the airfoil and the result in Fig. 9a has been obtained. Although the mean velocity field values are properly reproduced, the boundary layer still suffers an early detachment from the airfoil. In order to analyze in what extent the mesh element size, and not the formulation, was the reason for this discrepancy, the same problem has been run in a 2D section of the original profile using a much finer grid. Fig. 9b shows that the element size around the wall was indeed the cause of the early boundary layer detachment.

The same dependence on the mesh resolution can be found when capturing the acoustic modes. However, in this case the lack of accuracy does not affect the description of the acoustic scales generated by the interaction between the fluid and the airfoil, but its propagation to the far-field. The proper description of the wave requires dimensioning the element size at the far-field according to the smallest relevant wavelength, which would suppose an unaffordable problem size for a monolithic numerical approach. Fig. 10a shows how the wave propagation in the nearest region around the airfoil is not visible due to the presence of the much larger aerodynamic scale, but beyond a certain point it arises with the same pattern of the solution calculated with the FWH acoustic analogy in [48]. These challenges can only be approached with a manufactured structured mesh, which optimizes the spatial discretization according to the expected solution using elements with a high aspect ratio. Nevertheless, these methods are not part of the scope of the work.

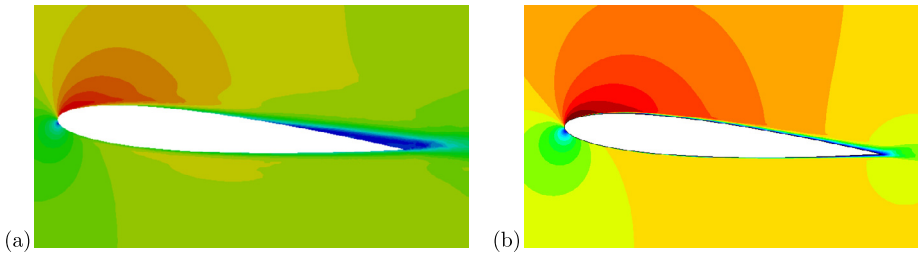

Fig. 9. Contours of time-averaged flow velocity calculated in a 3D domain (a), in a 2D domain (b) [48].

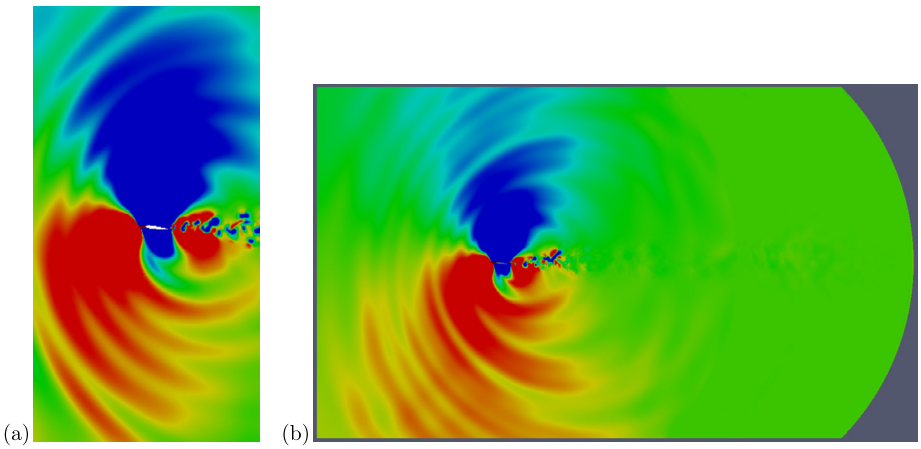

Fig. 10. Calculated total pressure at the near-field (a), at the far-field (b) [48].

The behavior of waves abandoning the domain is one of the main concerns in compressible flow calculations. In the previous case, due to the low Mach and Reynolds regime, the size of the near-field region under influence of the flow perturbations was very small compared to the domain size, for which the separated prescription of boundary conditions considering a mean flow component and an acoustic variation was conceptually very clear. However, in the present case real far-field stagnation conditions cannot be reached within a reasonably big domain and the aerodynamic pressure field is not yet uniform on the external boundaries, see Fig. 2. In spite of this theoretical drawback, the method manages to separate the two scales properly by updating the mean value at each time step, which allows the waves to cross Γ_L without any spurious reflection, see Fig. 10b. Furthermore, the implemented PML on the outlet completely absorbs the incoming waves as well as the noise produced by the airjet. It can be also observed how the flow pressure field is not exactly flat on Γ_L but no spurious reflections appear. This is possible because the present method is able to account for variations in the mean flow variables, but they must be smooth enough so they do not interfere with the acoustic field, otherwise spurious reflections may appear. Therefore, the truncation of the domain is not so immediate in this case since it must be assessed in advance that the far-field variations are acceptable, keeping always the computational cost in mind. It could be argued that this compromise could be avoided by using a PML on all external boundaries. Unfortunately this is only possible in solvers that compute the acoustic and the flow scales separately. In compressible formulations where the full set of variables is solved in a single calculation, like the present one, the inlet cannot be in contact with a PML. Moreover, the use of a global PML on all other external boundaries can lead to an unaffordable computational cost in big 3D cases with large wavelengths, for which the use of a non-radiating boundary condition has been prioritized.

5.3. Flow past an open cavity. $M = 0.7$

The acoustic feedback to the flow, which is one of the advantages of using unified solvers, has not been assessed yet. For this reason we next present a simulation of cavity noise. The case of a 2D flow past an open cavity ($M = 0.7$ and $Re = 41,000$) is considered. Periodic vortices are formed just downstream the leading edge of the cavity. When they impinge the trailing edge, an acoustic pulse is generated that propagates upstream and triggers flow instabilities, which result in flow separation at the leading edge. An acoustically driven feedback loop is thus established. We have compared the results to those provided by an equivalent DNS [49] for a more accurate and quantitative validation. This case is characterized by an inlet velocity $U = 245$ m/s and a rectangular cavity with a length $L = 5.18$ mm and a depth $D = 2.54$ mm. The mesh used to discretize the computational domain has $391,000$ linear elements and the time step size has been taken as 2×10^{-7}.

At M $= 0.7$ the acoustic scales are not negligible anymore respect to the flow oscillations like in the previous cases, and its feedback to the flow motion in the cavity becomes an important factor. This phenomenon affects in turn the subsequent

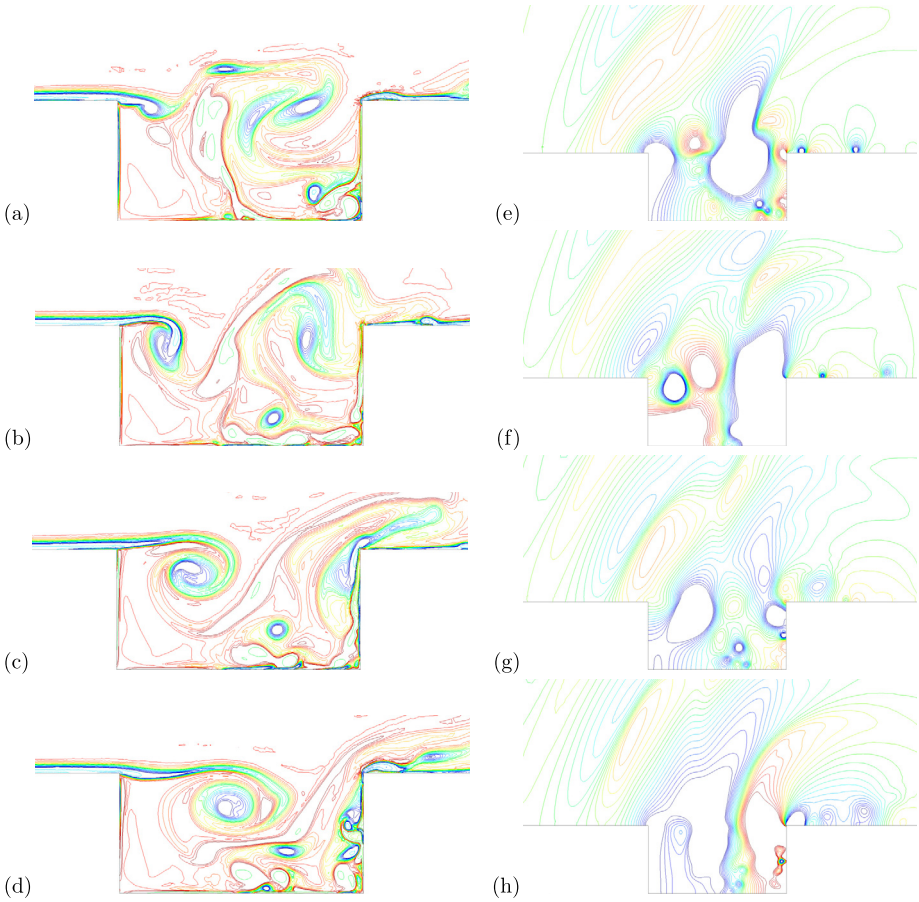

Fig. 11. Vorticity (a–d) and pressure (e–f) isosurfaces at four different moments during the main oscillation period [49].

wave propagation, for which it can be assumed that the coupling between scales is much stronger and the advantage of using a unified compressible solver is far more evident than in the two past scenarios. Fig. 11 shows vorticity and pressure isosurfaces in the cavity for four different times during a complete shedding period. These sequences can be directly compared to those presented in [49] because the same scaling has been used for both fields, and it can be concluded that the present formulation manages to reproduce the same flow patterns that were obtained with the DNS.

Unlike the previous open geometries, the partial confinement of the flow in the cavity increases the non-linearity of the problem because the propagation of the exiting waves is clearly affected by the unsteadiness of the flow. In this sense, Figs. 12 and 13 show that the acoustic component of the solution is also properly described by the isentropic solver. On the one hand, the main oscillation mode is found at the same Strouhal number $St = 0.68$ and a similar slope is obtained for the pressure frequency spectrum at the beginning of the acoustic region outside the cavity. On the other, the further wave propagation to the far field is also properly described by the present method, see Fig. 13 and [49].

6. Conclusions

The presented finite element formulation offers a simplified framework for dealing with subsonic adiabatic gas flows without facing the numerical inconveniences and the high computational cost of the state-of-the-art compressible flow formulations. The minimal implementation cost when departing from a monolithic incompressible solver makes this approach very attractive for solving aeroacoustic problems where heat transfer can be neglected. Moreover, its validation against the incompressible Navier–Stokes equations for a low-Mach regime has shown its suitability in problems where acoustics are not relevant. On the other hand, it has been also shown that the present formulation converges to a DNC when dealing with low speed flows.

The developed numerical method has successfully reproduced the acoustics of the incompressible Lighthill analogy and the FWH analogy with compressible flow, as well as the acoustic feedback to the flow of a DNS. The full subsonic range, from $M = 0.058$ to $M = 0.7$, has been covered and therefore, one of the main goals of this research, the development of a general numerical framework for all isentropic gas flows, has been successfully accomplished. In this sense, the presentation of a novel method for prescribing separate boundary conditions for the aerodynamic and the acoustic components strives

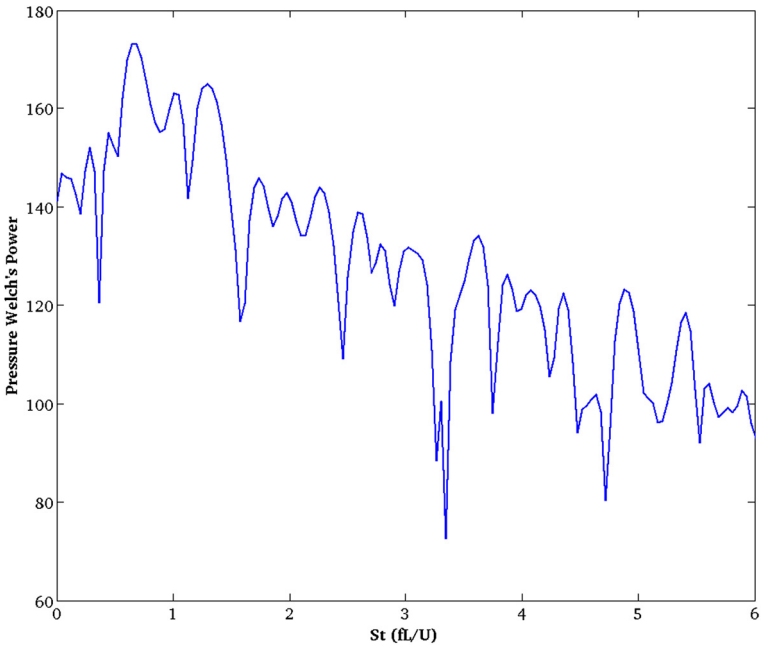

Fig. 12. Welch's power spectrum computed with the flow pressure field at the beginning of the acoustic region.

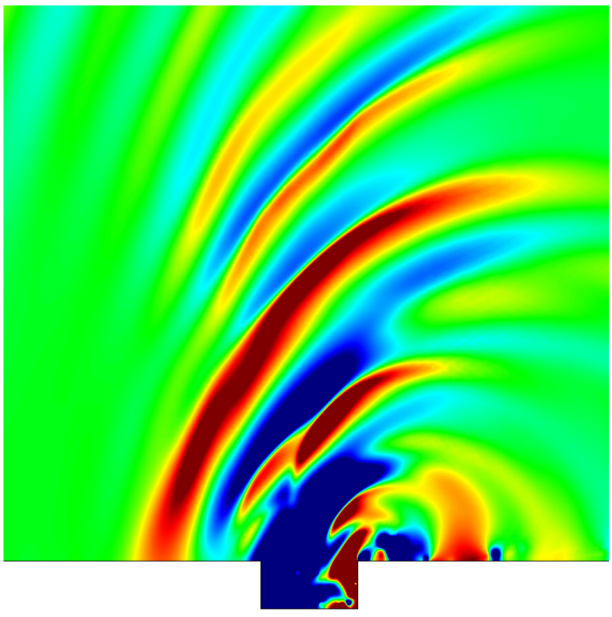

Fig. 13. Pressure wave propagation.

in the same direction of offering a general solution to the problem of spurious wave reflection in aeroacoustic calculations. On the most problematic boundary for such cases, the inlet, this formulation manages to prescribe an incoming velocity while being transparent to the exiting acoustic waves. Moreover, it is compatible with any kind of non-radiating boundary condition and can be combined with a PML on the outlet in case of highly convective jets.

Acknowledgements

The authors gratefully acknowledge the computer resources, technical expertise and assistance provided by the Red Española de Supercomputación (RES-BSC) and the financial support to CIMNE via the CERCA Programme/Generalitat de Catalunya. This work has been partially supported by the EU-FET grant EUNISON 308874. Moreover, the first author would also like to thank the Agència de Gestió d'Ajuts Universitaris i de Recerca for the predoctoral FI Grant no. 2015 FI-B 00227.

The second author gratefully acknowledges the support received from the Catalan Government through the ICREA Acadèmia Research Program and the third author acknowledges the support of the Spanish Government through the Ramón y Cajal grant RYC-2015-17367. The fourth author would like to gratefully acknowledge the support from the Secretaria d'Universitats i Recerca del Departament d'Economia i Coneixement (Generalitat de Catalunya) under grant 2014-SGR-0590, as well as the support of grant 2016-URL-IR-013 from the Generalitat de Catalunya and the Universitat Ramon Llull.

References

[1] A.J. Chorin, A numerical method for solving incompressible viscous flow problems, J. Comput. Phys. 2 (1) (1967) 12–26.
[2] D. Choi, C.L. Merkle, Application of time-iterative schemes to incompressible flow, AIAA J. 23 (10) (1985) 1518–1524.
[3] E. Turkel, Preconditioned methods for solving the incompressible and low speed compressible equations, J. Comput. Phys. 72 (2) (1987) 277–298.
[4] D.R. Durran, A physically motivated approach for filtering acoustic waves from the equations governing compressible stratified flow, J. Fluid Mech. 601 (2008) 365–379.
[5] C.A. Bayona Roa, J. Baiges, R. Codina, Variational multi-scale finite element approximation of the compressible Navier–Stokes equations, Int. J. Numer. Methods Heat Fluid Flow 26 (3/4) (2016) 1240–1271.
[6] C. Bailly, C. Bogey, O. Marsden, Progress in direct noise computation, Noise Notes 9 (3) (2010) 31–48.
[7] M.J. Lighthill, On sound generated aerodynamically I. General theory, Proc. R. Soc. Lond. Ser. A, Math. Phys. Sci. 211 (1107) (1952) 564–587.
[8] N. Curle, The influence of solid boundaries upon aerodynamic sound, Proc. R. Soc. Lond. Ser. A, Math. Phys. Sci. 231 (1187) (1955) 505–514.
[9] J.F. Williams, D.L. Hawkings, Sound generation by turbulence and surfaces in arbitrary motion, Philos. Trans. R. Soc. Lond. Ser. A, Math. Phys. Sci. 264 (1151) (1969) 321–342.
[10] J. Hardin, D. Pope, An acoustic/viscous splitting technique for computational aeroacoustics, Theor. Comput. Fluid Dyn. 6 (5–6) (1994) 323–340.
[11] W.Z. Shen, J.N. Sørensen, Aeroacoustic modelling of low-speed flows, Theor. Comput. Fluid Dyn. 13 (4) (1999) 271–289.
[12] C. Bogey, C. Bailly, D. Juvé, Computation of flow noise using source terms in linearized Euler equations, AIAA J. 40 (2) (2002) 235–243.
[13] C. Bailly, D. Juve, Numerical solution of acoustic propagation problems using linearized Euler equations, AIAA J. 38 (1) (2000) 22–29.
[14] J.H. Seo, Y.J. Moon, Linearized perturbed compressible equations for low Mach number aeroacoustics, J. Comput. Phys. 218 (2) (2006) 702–719.
[15] R. Ewert, W. Schröder, Acoustic perturbation equations based on flow decomposition via source filtering, J. Comput. Phys. 188 (2) (2003) 365–398.
[16] M. Kaltenbacher, S. Zörner, A. Hüppe, P. Sidlof, 3d numerical simulations of human phonation, in: Proceedings of the 11th World Congress on Computational Mechanics-WCCM XI, 2014.
[17] O. Guasch, P. Sánchez-Martín, A. Pont, J. Baiges, R. Codina, Residual-based stabilization of the finite element approximation to the acoustic perturbation equations for low Mach number aeroacoustics, Int. J. Numer. Methods Fluids 82 (12) (2016) 839–857.
[18] M. Roger, The acoustic analogy, some theoretical background, Lect. Ser. - Kareman Inst. Fluid Dyn. 2 (2000) A1–A32.
[19] O. Guasch, A. Pont, J. Baiges, R. Codina, Concurrent finite element simulation of quadrupolar and dipolar flow noise in low Mach number aeroacoustics, Comput. Fluids 133 (2016) 129–139.
[20] R. Codina, J. Baiges, Weak imposition of essential boundary conditions in the finite element approximation of elliptic problems with non-matching meshes, Int. J. Numer. Methods Eng. 104 (7) (2015) 624–654.
[21] H. Espinoza, R. Codina, S. Badia, A Sommerfeld non-reflecting boundary condition for the wave equation in mixed form, Comput. Methods Appl. Mech. Eng. 276 (2014) 122–148.
[22] E. Vergnault, O. Malaspinas, P. Sagaut, Noise source identification with the lattice Boltzmann method, J. Acoust. Soc. Am. 133 (3) (2013) 1293–1305.
[23] O. Colomés, S. Badia, R. Codina, J. Principe, Assessment of variational multiscale models for the large eddy simulation of turbulent incompressible flows, Comput. Methods Appl. Mech. Eng. 285 (2015) 32–63.
[24] O. Guasch, R. Codina, Statistical behavior of the orthogonal subgrid scale stabilization terms in the finite element large eddy simulation of turbulent flows, Comput. Methods Appl. Mech. Eng. 261 (2013) 154–166.
[25] P.H. Oosthuizen, W.E. Carscallen, Introduction to Compressible Fluid Flow, CRC Press, 2013.
[26] M. Avila, J. Principe, R. Codina, A finite element dynamical nonlinear subscale approximation for the low Mach number flow equations, J. Comput. Phys. 230 (22) (2011) 7988–8009.
[27] P. Fosso, H. Deniau, N. Lamarque, T. Poinsot, et al., Comparison of outflow boundary conditions for subsonic aeroacoustic simulations, Int. J. Numer. Methods Fluids 68 (10) (2012) 1207–1233.
[28] V. Granet, O. Vermorel, T. Léonard, L. Gicquel, T. Poinsot, Comparison of nonreflecting outlet boundary conditions for compressible solvers on unstructured grids, AIAA J. 48 (10) (2010) 2348–2364.
[29] K.W. Thompson, Time dependent boundary conditions for hyperbolic systems, J. Comput. Phys. 68 (1) (1987) 1–24.
[30] T.J. Poinsot, S. Lele, Boundary conditions for direct simulations of compressible viscous flows, J. Comput. Phys. 101 (1) (1992) 104–129.
[31] R. Prosser, Improved boundary conditions for the direct numerical simulation of turbulent subsonic flows I. Inviscid flows, J. Comput. Phys. 207 (2) (2005) 736–768.
[32] R. Prosser, Towards improved boundary conditions for the DNS and LES of turbulent subsonic flows, J. Comput. Phys. 222 (2) (2007) 469–474.
[33] C.S. Yoo, H.G. Im, Characteristic boundary conditions for simulations of compressible reacting flows with multi-dimensional, viscous and reaction effects, Combust. Theory Model. 11 (2) (2007) 259–286.
[34] J.-P. Berenger, A perfectly matched layer for the absorption of electromagnetic waves, J. Comput. Phys. 114 (2) (1994) 185–200.
[35] F.Q. Hu, A perfectly matched layer absorbing boundary condition for linearized Euler equations with a non-uniform mean flow, J. Comput. Phys. 208 (2) (2005) 469–492.
[36] C.K. Tam, Z. Dong, Radiation and outflow boundary conditions for direct computation of acoustic and flow disturbances in a nonuniform mean flow, J. Comput. Acoust. 4 (02) (1996) 175–201.
[37] C. Bogey, C. Bailly, Three-dimensional non-reflective boundary conditions for acoustic simulations: far field formulation and validation test cases, Acta Acust. Acust. 88 (4) (2002) 463–471.
[38] M. Juntunen, R. Stenberg, Nitsche's method for general boundary conditions, Math. Comput. 78 (267) (2009) 1353–1374.
[39] R. Codina, J. Baiges, Approximate imposition of boundary conditions in immersed boundary methods, Int. J. Numer. Methods Eng. 80 (11) (2009) 1379–1405.
[40] H. Takemoto, P. Mokhtari, T. Kitamura, Acoustic analysis of the vocal tract during vowel production by finite-difference time-domain method, J. Acoust. Soc. Am. 128 (6) (2010) 3724–3738.
[41] T.J. Hughes, G.R. Feijóo, L. Mazzei, J.-B. Quincy, The variational multiscale method. A paradigm for computational mechanics, Comput. Methods Appl. Mech. Eng. 166 (1–2) (1998) 3–24.
[42] R. Codina, On stabilized finite element methods for linear systems of convection–diffusion–reaction equations, Comput. Methods Appl. Mech. Eng. 188 (1) (2000) 61–82.

[43] R. Codina, S. Badia, J. Baiges, J. Principe, Variational Multiscale Methods in Computational Fluid Dynamics, Encyclopedia Comput. Mech., John Wiley & Sons Ltd., 2018.
[44] R. Codina, Stabilized finite element approximation of transient incompressible flows using orthogonal subscales, Comput. Methods Appl. Mech. Eng. 191 (39) (2002) 4295–4321.
[45] R. Codina, J. Principe, O. Guasch, S. Badia, Time dependent subscales in the stabilized finite element approximation of incompressible flow problems, Comput. Methods Appl. Mech. Eng. 196 (21) (2007) 2413–2430.
[46] O. Guasch, R. Codina, An algebraic subgrid scale finite element method for the convected Helmholtz equation in two dimensions with applications in aeroacoustics, Comput. Methods Appl. Mech. Eng. 196 (45) (2007) 4672–4689.
[47] C. Bayona, J. Baiges, R. Codina, Solution of low Mach number aeroacoustic flows using a variational multi-scale finite element formulation of the compressible Navier–Stokes equations written in primitive variables, submitted for publication.
[48] W.R. Wolf, S.K. Lele, Trailing edge noise predictions using compressible les and acoustic analogy, in: Proceedings of the 17th AIAA/CEAS Aeroacoustics Conference, AIAA Paper, vol. 2784, 2011, pp. 1–25.
[49] X. Gloerfelt, C. Bailly, D. Juve, Computation of the noise radiated by a subsonic cavity using direct simulation and acoustic analogy, AIAA paper 2226 (7).